AIAA JOURNAL
Vol. 38, No. 12, December 2000

Computation of Trailing-Edge Flow and Noise Using Large-Eddy Simulation

Meng Wang* and Parviz Moin†
Stanford University, Stanford, California 94305

Turbulent boundary layers near the trailing edge of a lifting surface are known to generate intense, broadband scattering noise as well as surface pressure fluctuations. Numerically predicting the trailing-edge noise requires that the noise-generating eddies over a wide range of length scales be adequately represented. The large-eddy simulation (LES) technique provides a promising tool for obtaining the unsteady wall-pressure fields and the acoustic source functions. An LES is carried out for turbulent boundary-layer flow past an asymmetrically beveled trailing edge of a flat strut at a chord Reynolds number of 2.15×10^6. The computed velocity and surface pressure statistics compare reasonably well with previous experimental measurements. The far-field acoustic calculation is facilitated by the integral solution to the Lighthill equation derived by Ffowcs-Williams and Hall. Computations have been carried out to determine the far-field noise spectra, the source-term characteristics, and the requirement for the integration domain size. It is found that the present LES domain is adequate for predicting noise radiation over a range of frequencies. At the low-frequency end, however, the spanwise source coherence estimated based on surface pressure fluctuations does not decay sufficiently, suggesting the need for a wider computational domain.

I. Introduction

THE aeroacoustics of flow–airfoil interaction exhibit distinct characteristics depending on the physical length scales involved. In the small-body (relative to acoustic wavelength) limit characteristic of the noise generated by large-scale vortex shedding at low flow Mach numbers, the noise calculation is facilitated by the use of Lighthill's analogy[1] in conjunction with a free-space Green's function, in the sense of Curle's formulation[2] (or more generally, the Ffowcs-Williams and Hawkings equation[3]). Computations using this approach can be found in, for example, Refs. 4 and 5.

A more fascinating aspect of airfoil noise is the aeroacoustic scattering by the trailing edge. This occurs at the large-body limit (i.e., when the chord is comparable with or exceeds the acoustic wavelength) and is the source of intense broadband noise.[6,7] The presence of a sharp trailing edge enhances radiation to the far field by altering the source characteristics; for instance, turbulent eddies, known as quadrupole source in free space, behave in a nonmultipole (sometimes termed $\frac{3}{2}$-pole) fashion in the vicinity of a semi-infinite flat-plate edge.[8,9] To account for the surface reflection of acoustic waves, a hard-wall Green's function must be employed in an integral solution to the Lighthill equation[1] if the acoustic source terms are obtained from incompressible flow solutions under low Mach number approximation. If the source field is obtained from a compressible flow simulation and contains accurate acoustic information, the free-space Green's function is applicable, and the Ffowcs-Williams and Hawkings equation[3] provides a convenient framework for solving this class of problems.[10] Howe[11] gave an extensive review of the theoretical developments in trailing edge noise prediction methods.

In addition to the direct noise radiation, the surface-pressure fluctuations (pseudo-sound) are of importance because they tend to excite structural vibration and low-frequency noise.[12] The rapid changes in surface pressure near the trailing edge provide an efficient mechanism for generating the detrimental lower-frequency content of the wall-pressure wave number spectrum. The problem is often further complicated by the presence of adverse pressure gradient, boundary-layer separation, and vortex shedding in the trailing-edge region.

To predict the trailing-edge noise numerically, the noise-generating eddies over a wide range of length scales must be adequately represented. This requirement cannot be met by the traditional computational fluid dynamics methods based on Reynolds-averaged Navier–Stokes (RANS) equations or Euler equations. A large-eddy simulation (LES) technique provides a promising tool for obtaining the unsteady surface-pressure fields and the near-field turbulence quantities. LES is well suited for computing the noise source at Reynolds numbers of engineering interest because it resolves only the energy-containing eddies, known to be significant contributors to noise radiation. The effect of small (subgrid) scale eddies on the large- (resolved) scale motion is modeled, thus drastically reducing the computational cost as compared with direct numerical simulation (DNS).

The present work is aimed at developing numerical prediction methods for trailing-edge aeroacoustics using a combination of LES and Lighthill's theory.[1] The instantaneous turbulent flowfield near the trailing edge is obtained by means of LES based on the incompressible Navier–Stokes equations. The space–time evolution of the surface-pressure fluctuations, useful as forcing function for structural vibration models, is also computed directly. The simulation results allow the acoustic source functions, or the fluctuating Reynolds stresses, to be evaluated. The radiated noise is then computed from an integral-form solution to the Lighthill equation using an approximate hard-wall Green's function (see Ref. 8). This approach has recently been employed by Manoha et al.[13] to predict the vortex shedding noise from essentially laminar boundary layers interacting with a rectangular trailing edge. The present work focuses on the broadband noise of realistic turbulent boundary layers incident on a sharp, asymmetric trailing edge at a Reynolds number much higher than that considered in Ref. 13.

The case under study corresponds to the experiment conducted by Blake.[14] As shown in Fig. 1, a two-dimensional flat strut with a circular leading edge and an asymmetric, beveled trailing edge of 25-deg tip angle is placed in a uniform stream at a 0-deg angle of attack. The strut's chord $C = 21.125h$, and span $L = 23.5h$, where h is the thickness. The Reynolds number based on freestream velocity U_∞ and the chord is 2.15×10^6. The free-stream Mach number $M = U_\infty / c_\infty \approx 0.088$. This flow is particularly interesting in that the asymmetric edge shape produces a separated flow on the low-pressure side and an attached boundary layer on the high-pressure side, thus creating complex shear layer interactions in the vicinity of the trailing edge. B, C, D, E, F, and G indicate measurement stations in Blake's experiment.[14] They are located at $x_1/h = -4.625$,

Received 24 February 1999; revision received 23 February 2000; accepted for publication 16 June 2000.

*Senior Research Associate, Center for Turbulence Research, Stanford University/NASA Ames Research Center, MS 202A-1, Moffett Field, CA 94035.

†Franklin and Caroline Johnson Professor of Engineering, Department of Mechanical Engineering; also Senior Staff Scientist, NASA Ames Research Center, Moffett Field, CA 94035. Associate Fellow AIAA.

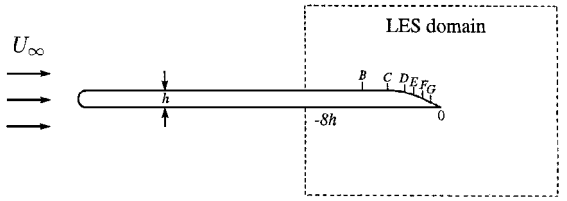

Fig. 1 Flow configuration and computational domain; experimental measurement stations B–G are located at $x_1/h = -4.625, -3.125, -2.125, -1.625, -1.125$, and -0.625, respectively.

-3.125, -2.125, -1.625, -1.125, and -0.625, respectively, in a Cartesian coordinate system originating from the trailing edge. Statistical measurements of velocity and fluctuating surface pressure fields in the trailing-edge region are available for comparison with computational results. Acoustic measurements were not made in this experiment, although they were made in a separate experiment[7] under different flow conditions, using trailing edges similar, but not identical, to the one in Fig. 1.

II. LES of Trailing-Edge Flow

A. Computational Methodology

The near-field LES solves the spatially filtered, unsteady, incompressible Navier–Stokes equations in conjunction with the dynamic subgrid-scale (SGS) model.[15,16] The numerical code is an adaptation of the C-grid code described by Choi[17] and Mittal.[18] Spatial discretization is achieved using second-order central differences in the streamwise and wall-normal directions and Fourier collocation in the spanwise direction. The time advancement is of the fractional step type, in combination with the Crank–Nicolson method for viscous terms and third-order Runge–Kutta scheme for convective terms. The continuity constraint is imposed through a pressure Poisson equation, solved at each Runge–Kutta substep using a multigrid iterative procedure.

To reduce the computational cost while capturing the essential physical processes of interest, simulations are conducted in a computational domain containing the aft section of the strut and the near wake, as illustrated in Fig. 1. Except for the inlet, the other three sides of the domain have been truncated for clarity. The actual domain size is approximately $16.5h$, $41h$, and $0.5h$, in the streamwise, x_1, wall normal, x_2, and spanwise x_3 directions, respectively. The computational grid, defined in curvilinear coordinates in the x_1–x_2 plane and Cartesian coordinate in x_3, uses a total of $1536 \times 96 \times 48$ points, with appropriate clustering in the near-wall and trailing-edge regions. Of the 1536 streamwise grid points, 640 are distributed along the upper surface, 512 along the lower surface, and 2×192 along the wake line (branch cut). The maximum grid spacing along the strut surface, measured in wall units, is $\Delta x_1^+ \approx 62$, $\Delta x_3^+ \approx 55$, and $\Delta x_2^+ \approx 2$. The simulation, running at a maximum Courant–Friedrichs–Lewy number of 1.5, requires 200 single processor CPU hours on CRAY C90 to advance one flow time across the streamwise domain length, and over 1000 CPU hours for the complete simulation. The velocity and pressure statistics presented hereafter are collected over a period $T_s U_\infty / h \approx 60.62$, or 3.67 flow-through times based on freestream velocity.

The boundary conditions at the inlet are obtained by the following procedure. First, an auxiliary RANS calculation is conducted in a C-grid domain enclosing the entire strut, using Menter's shear-stress transport (SST) k–ω model.[19] The resulting mean velocities, accounting for the flow acceleration and circulation associated with a lifting surface, are used as the inflow profiles outside the boundary layers on both sides of the strut. Within the turbulent boundary layers the time series of inflow velocities are generated from two separate LES of flat-plate boundary layers with zero pressure gradient, using the method described by Lund et al.[20] The inflow-generation LES employs an identical mesh resolution as for the trailing-edge flow LES at the inlet and matches the local boundary-layer properties, including the momentum thickness and Reynolds number, with those from the RANS simulation.

A no-slip condition is applied on the surface of the strut. The top and bottom boundaries are placed far ($\sim 20h$) away from the strut to minimize the impact of the imposed velocities, obtained from RANS calculations. At the downstream boundary, the convective outflow condition[21] is applied to allow the vortical disturbances in the wake to leave the computational domain smoothly.

The present numerical method and the computer program have been validated in the LES of several turbulent flows, including flow past a circular cylinder[22] and flow in a planar asymmetric diffuser.[23] The same code has also been used to perform the trailing-edge flow LES in conjunction with wall-layer models on a coarser grid (one-sixth of the present grid size),[24] and good agreement with the present full LES solutions has been obtained.

B. Simulation Results

Figure 2a depicts contours of the instantaneous streamwise velocity u_1/U_∞ at a given spanwise location. The mean streamwise velocity (U_1/U_∞) contours, obtained by averaging over the homogeneous spanwise direction and time, are plotted in Fig. 2b. Note that the numerically simulated fields exhibit realistic turbulence structures and a small separated zone near the trailing edge. The two shear layers, arising from the separated boundary layer on the upper side and the attached boundary layer on the lower side, interact to produce a turbulent wake in the downstream direction. No coherent vortex shedding is observed, in agreement with Blake's experimental data,[14] which show vortex shedding from a 45-deg trailing edge but not the 25-deg one.

In Fig. 3, the magnitude of the mean velocity $U = (U_1^2 + U_2^2)^{1/2}$ normalized by its value at the boundary-layer edge U_e is plotted as

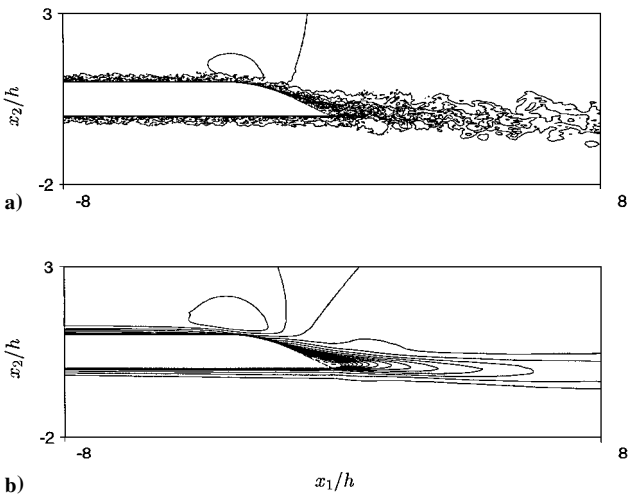

Fig. 2 Velocity fields computed from LES: a) instantaneous streamwise velocity u_1/U_∞ at a given spanwise cut (contour levels from -0.236 to 1.274, with increment 0.116) and b) mean streamwise velocity U_1/U_∞ (contour levels from -0.081 to 1.207, with increment 0.068).

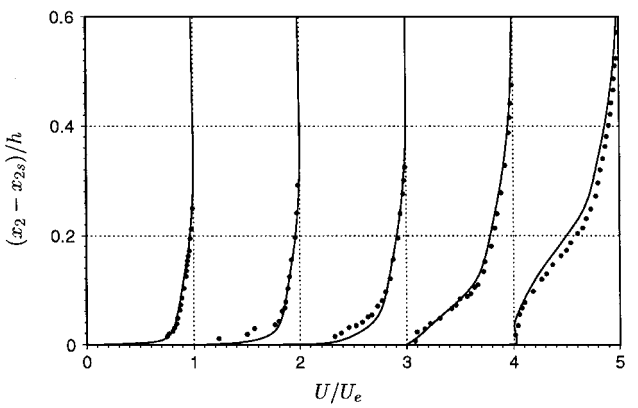

Fig. 3 Profiles of the normalized mean velocity magnitude as a function of vertical distance from the upper surface, at stations (from left to right) C, D, E, F, and G: ——, LES, and ●, Blake's experiment[14]; individual profiles are separated by a horizontal offset of 1 with the corresponding zero lines located at 0, 1, . . . , 4.

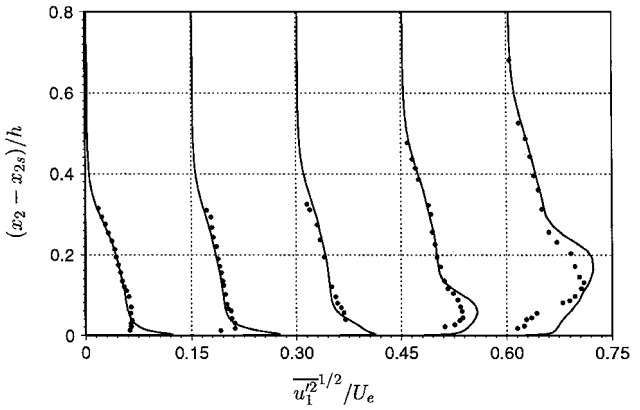

Fig. 4 Profiles of the rms streamwise velocity fluctuations as a function of vertical distance from the upper surface, at stations (from left to right) *B*, *D*, *E*, *F*, and *G*: ——, LES, and ●, Blake's experiment[14]; individual profiles are separated by a horizontal offset of 0.15 with the corresponding zero lines located at 0, 0.15, . . . , 0.60.

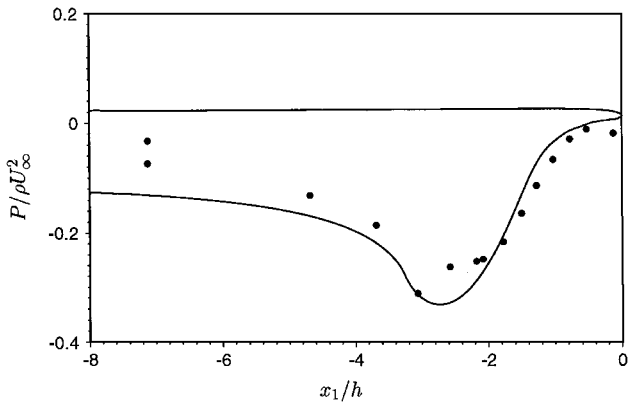

Fig. 5 Mean surface pressure distribution near the trailing edge: ——, LES, and ●, Blake's experiment.[14]

a function of vertical distance from the upper surface at streamwise stations (from left to right) *C*–*G*. The solid lines are from LES, and the symbols represent Blake's[14] experimental data. Good agreement with the experimental results is obtained at station *C* and all of the upstream locations. At stations *D* and *E*, where the boundary layer is subject to strong adverse pressure gradient but remains attached to the wall, the LES profiles are fuller in the near-wall region than those from the experiment. Farther downstream, as an unsteady separated region develops, the discrepancy diminishes, and the computed profiles compare well again with the experimental results at stations *F* and *G*.

Figure 4 compares the computational and experimental profiles of the rms streamwise velocity fluctuations at stations (from left to right) *B*, *D*, *E*, *F*, and *G*. The agreement between the LES and the experimental results is quite good except in the near-wall region and at the last two stations. The experimental profiles are seen to miss consistently the near-wall peaks known to exist in turbulent boundary layers, suggesting a possible lack of spatial resolution or high-frequency response as the probe approaches the wall. The large discrepancy observed in the separated region (stations *F* and *G*) may be caused by both simulation and measurement errors. In general, hot-wire readings become increasingly difficult to interpret if the rms turbulence intensity exceeds 30% of the local mean velocity,[25] which is the case in the separation bubble where the mean velocity is very small (cf. Fig. 3).

The dimensionless mean pressure ($=C_p/2$) is depicted in Fig. 5 as a function of x_1. The comparison between the LES and experimental results is reasonable in the trailing-edge region, but unsatisfactory upstream of it. The experimental data plotted here were provided in a private communication by W. K. Blake in 1998 after the completion of the present LES. Only a single datum point is available on the lower surface (the upper point at $x_1/h = -7.125$).

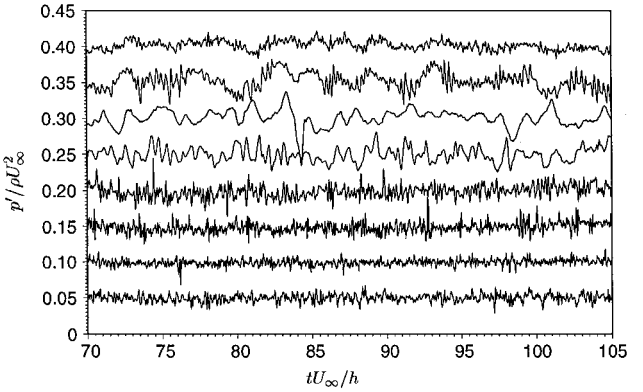

Fig. 6 Time history of surface pressure fluctuations at streamwise stations (from bottom to top) *B*, *C*, *D*, *E*, *F*, *G*, trailing edge, and *G* (lower surface), at a fixed spanwise coordinate; individual curves are separated by a vertical offset of 0.05 with the corresponding zero lines located at 0.05, 0.10, . . . , 0.40.

Based on this point, and assuming that the mean pressure is approximately constant on the lower surface as suggested by the LES prediction, it is evident that the lift and, hence, circulation in the experiment are much smaller than those in the LES. Because the circulation in the LES is imposed through the unequal mean velocity profiles on the two sides of the strut at the inlet boundary, one concludes that the difference between the inflow velocities, provided by the auxiliary RANS calculation, has been exaggerated. Indeed, an estimate using C_p and the Bernoulli equation indicates that, in the experiment, the inflow velocities at the boundary layer edges are $U_e^{\text{upper}} \approx 1.071U_\infty$ and $U_e^{\text{lower}} \approx 1.032U_\infty$, compared with $U_e^{\text{upper}} \approx 1.093U_\infty$ and $U_e^{\text{lower}} \approx 0.979U_\infty$ used in the LES.

Temporal variations of wall-pressure fluctuations are exemplified in Fig. 6. The curves are obtained at stations (from bottom to top) *B*–*G*, the trailing edge, and *G* on the lower surface, at a fixed spanwise location. At stations *B*–*E* the pressure signals consist of predominantly high-frequency fluctuations associated with small-scale eddies in the attached turbulent boundary layer. The oscillation amplitude is decreased in the favorable pressure gradient region (station *C*) and increased in the adverse pressure gradient region (stations *D* and *E*). After the boundary layer is separated (stations *F* and *G*), the high-frequency content is diminished, and the surface pressure is characterized by lower-frequency and higher-amplitude oscillations caused by the unsteady separation. The high-frequency content reappears at the trailing edge owing to the contribution from the attached turbulent boundary layer on the lower side. Meanwhile, the influence of the unsteady separation and wake extends upstream from the trailing edge on the lower surface, as evidenced by the low-frequency content visible in the top curve (position *G* on lower surface). This influence diminishes gradually as one moves farther upstream.

Figure 7 shows the space–time correlations of the upper-surface pressure fluctuations as a function of temporal and spanwise separations at stations *C*–*G* and the trailing edge (actually, one-half grid spacing from the edge on the staggered mesh). The isocorrelation contours show relatively small variations of the spanwise spatial and temporal scales from stations *C* to *E*, underneath the attached boundary layer with adverse pressure gradient. A dramatic increase of spatial and temporal scales occurs, however, after the turbulent boundary layer becomes separated (stations *F*, *G*, and the trailing edge). The wall pressure fluctuations inside the separated zone are dominated by the effect of large-scale fluid motion. The small-scale eddies from the upstream boundary layer are lifted away from the wall, and, hence, their contribution to the wall pressure is diminished, as is evident in Fig. 6. At the trailing edge, the correlation contours exhibit some features of small-scale correlation superimposed on the extremely large overall scales because of the contribution from the lower-surface boundary layer.

Note that the correlation contours in Fig. 7 show insufficient drop at maximum spanwise separations inside the separated region, particularly at station *G* and the trailing edge. This suggests that the

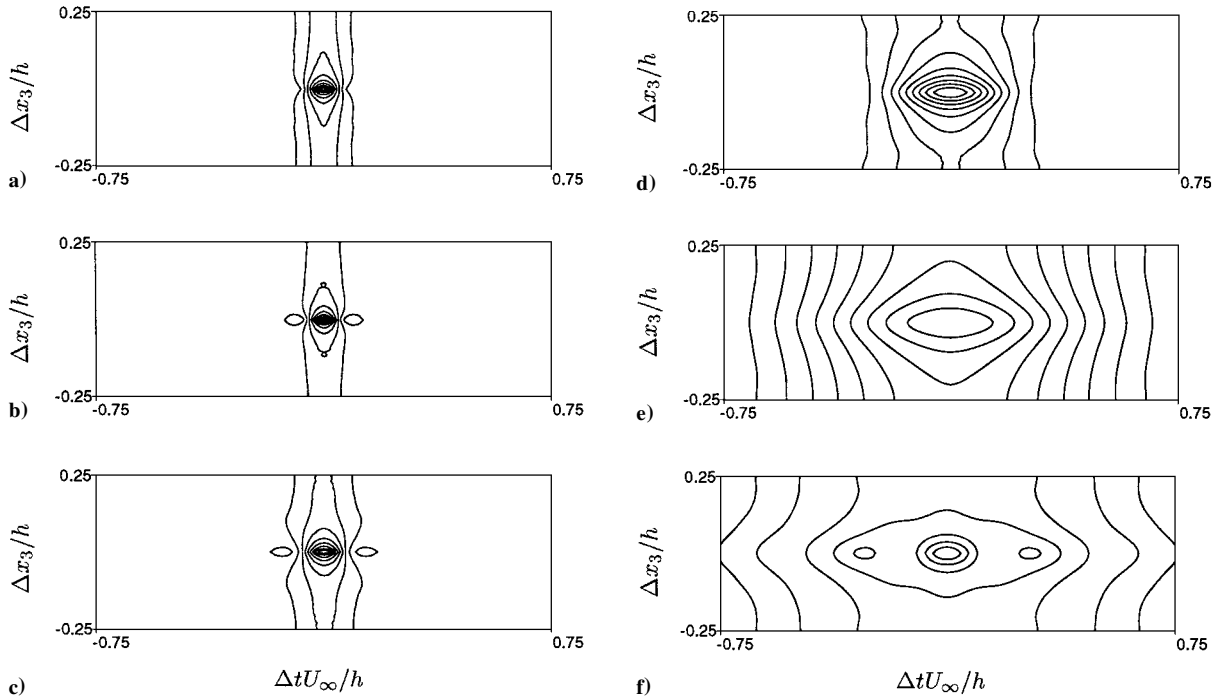

Fig. 7 Contours of space–time correlation of the upper-surface pressure fluctuations as a function of spanwise and temporal separations, at stations a) *C*, b) *D*, c) *E*, d) *F*, e) *G*, and f) trailing edge; contour values are from 0.1 to 0.9, with increment 0.1.

computational domain is too restrictive in the spanwise direction to allow the development of fully three-dimensional large-scale flow structures. The effect of the small spanwise domain size on the low-order flow statistics described has not been investigated. In addition, spanwise domain size has important implications to the acoustic prediction, as will be discussed in Sec. III.

Figure 8 depicts the frequency spectra of wall pressure fluctuations calculated from LES and compares them with those from Blake's experiment.[14] The variables used for normalization are U_∞, h, and the dynamic pressure $q_\infty = \rho U_\infty^2/2$. The calculated spectra agree relatively well with the experimental data at most stations except station G, where the spectrum is significantly overpredicted. Note that before the boundary-layer separation (stations C–E), the LES spectra drop off more quickly than the experimental spectra at the high-frequency end due to limited grid resolution and finite difference errors. The high-frequency content corresponds to fine spatial structures not resolved on the simulation grid. After the separation, however, the small-scale effect is diminished, and the LES is capable of capturing the entire frequency range measured by the experiment. The spectrum at the trailing edge, where no experimental data are available, again consists of contributions from the upper (separated) and lower (attached) boundary layers. The latter is responsible for the high-frequency peak shown in Fig. 8f.

III. Noise Computation

A. Overview of Methods

The noise radiation to the far field is calculated in the framework of Lighthill's theory.[1] Crighton and Leppington[9] show that the trailing-edge noise field has a nonmultipole character, which is caused by the scattering surface being noncompact relative to the acoustic wavelength. To account for the surface reflection, the correct boundary conditions must be satisfied by both hydrodynamic and acoustic components of the flow. This can be achieved in two ways, depending on the information contained within the available source-field data.

If the source field is computed from the incompressible Navier–Stokes equations, as in the present study, a hard-wall Green's function, whose normal derivative vanishes on the surface, must be employed in an integral solution to the Lighthill equation to impose the acoustic wall condition. The convolution of source terms with the geometry-specific Green's function causes the disturbance wave numbers to be converted from the hydrodynamic domain to the acoustic domain. An important advantage of this method is that the source structure, for example, the "$\frac{3}{2}$-pole" for a thin-plate edge, is correctly represented. This is crucial in acoustic-analogy-based calculations because a mischaracterization of the acoustic source can cause numerical errors to overwhelm the predicted noise. Another advantage of using the specific Green's function is that only incompressible source functions are required. Incompressible turbulence is less costly to simulate numerically than compressible turbulence. The drawback of this method is that the exact Green's function is not in general available in closed form. It has to be approximated or computed numerically.

If, on the other hand, the source field is obtained from the compressible Navier–Stokes equations, the hard-wall boundary condition is automatically satisfied by both the hydrodynamic and acoustic components, and a free-space Green's function may be used. The integral solutions of Curle[2] and Ffowcs-Williams and Hawkings[3] provide a useful framework. The Ffowcs-Williams and Hawkings equation is the most general form of integral solutions to the Lighthill equation, allowing for arbitrary surface velocity. At low Mach numbers the solution is considered to be dominated by the surface terms in apparent monopole and dipole forms, and the true noise characteristics emerges only if the numerical integration accurately accounts for the constructive/destructive interferences among signals from the noncompact surface elements. Singer et al.[10] used this approach in conjunction with a compressible flow solver to compute the sound of two-dimensional vortices convected past the trailing edge of a thin airfoil. The calculation was shown to capture the basic features of edge-scattering noise, and the discrepancies with theory (the two-dimensional version of Ffowcs-Williams and Hall's[8] half-plane solution) were explained in terms of the finite chord effect and the nonlinear scaling of the rms velocity fluctuations near the trailing edge with the freestream velocity.

B. Formulation and Approximations

When the acoustic wavelength is much longer than the thickness of the strut but much shorter than the chord ($h \ll \lambda_a \ll C$), which covers an important range of frequencies (to be noted later), the strut is reasonably approximated by a semi-infinite plane with zero thickness. Crighton and Leppington[9] and Howe[26,27] demonstrate analytically that in the acoustically thin foil limit, the specific trailing-edge shape does not affect the fundamental scattering properties such as

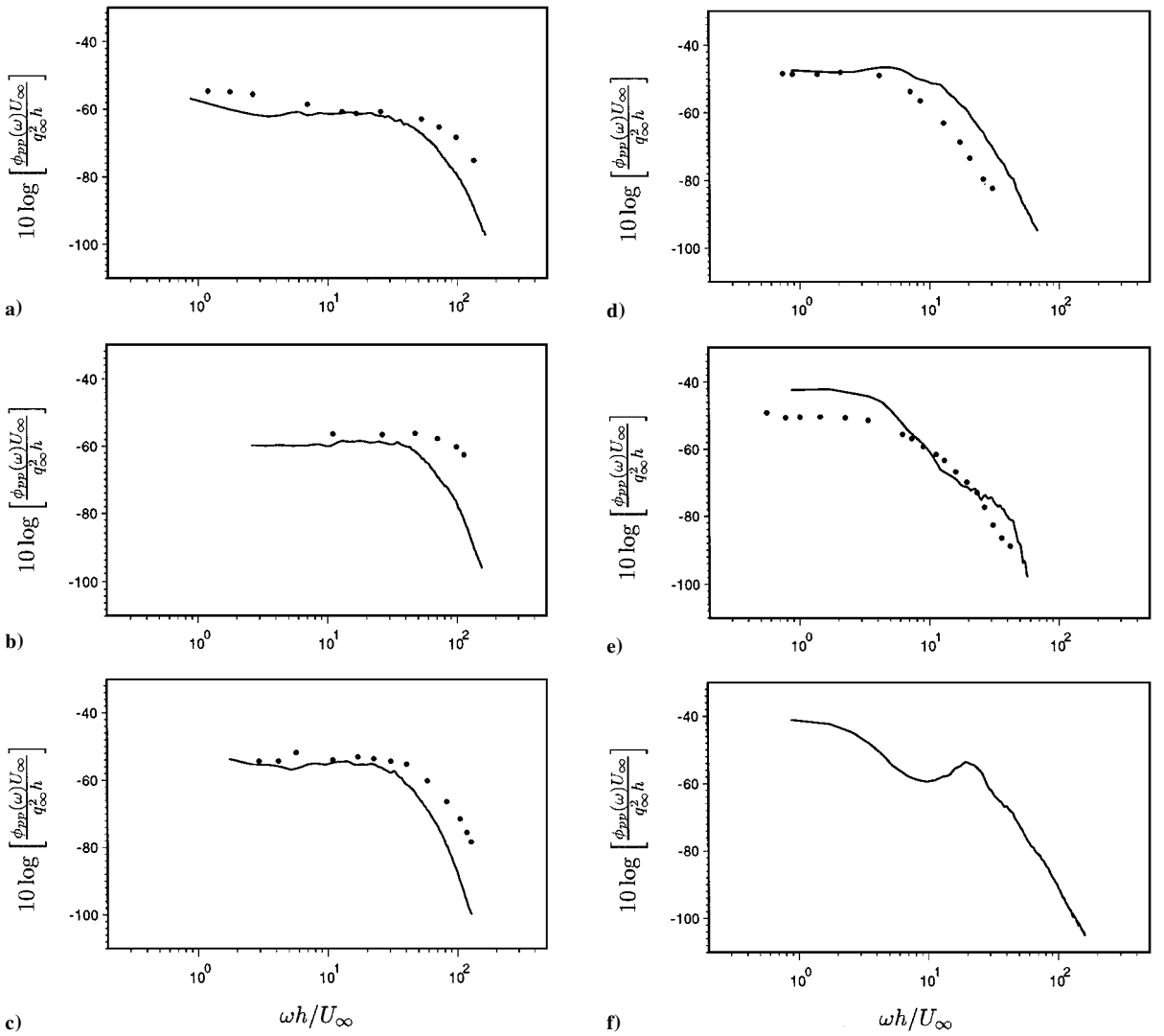

Fig. 8 Frequency spectra of wall pressure fluctuations at stations a) *C*, b) *D*, c) *E*, d) *F*, e) *G*, and f) trailing edge: ——, LES, and ●, experiment.

the directivity and the velocity scaling of the predicted noise spectra. By using the thin half-plane Green's function, Ffowcs-Williams and Hall[8] show that the far-field pressure perturbation in the frequency domain can be written in the form

$$\hat{p}_a(\boldsymbol{x},\omega) \approx \frac{2e^{-i(\pi/4)}}{\pi^{\frac{1}{2}}} k^2 \sin\frac{\theta}{2} \int_V \frac{e^{ikR}}{4\pi R} \frac{(\sin\phi)^{\frac{1}{2}}}{(2kr_0)^{\frac{3}{2}}} \times \left\{ \rho_\infty \left(\widehat{u_\theta^2} - \widehat{u_r^2}\right) \sin\frac{\theta_0}{2} - 2\rho_\infty \widehat{u_r u_\theta} \cos\frac{\theta_0}{2} \right\} \mathrm{d}^3\boldsymbol{y} \qquad (1)$$

where the caret denotes temporal Fourier transform, ω is the circular frequency, and $k = \omega/c_\infty$ is the acoustic wave number. The velocity components u_r and u_θ are defined in a cylindrical-polar coordinate system shown in Fig. 9. Position vectors $\boldsymbol{x}$ (r, θ, z) and $\boldsymbol{y}$ (r_0, θ_0, z_0) represent far-field and source-field points, respectively, with $R = |\boldsymbol{x} - \boldsymbol{y}|$ and $\sin\phi = r/[r^2 + (z - z_0)^2]^{1/2}$.

In addition to the approximate Green's function, several assumptions are implied in Eq. (1). The viscous stress is assumed unimportant as a noise source at high Reynolds numbers. The convection, refraction, and scattering of acoustic waves by the turbulent flow are ignored, which is justifiable in the low-Mach-number limit except at very high frequencies and/or at θ values close to 0 or π. Furthermore, the integrand in Eq. (1) is derived for a source region well within one acoustic wavelength from the trailing edge ($kr_0 \ll 1$ or $r_0 \ll \lambda_a$). Although only eddies within this distance contribute to the amplified scattering noise, from a computational point of view, it is desirable to integrate farther out for better convergence (boundary

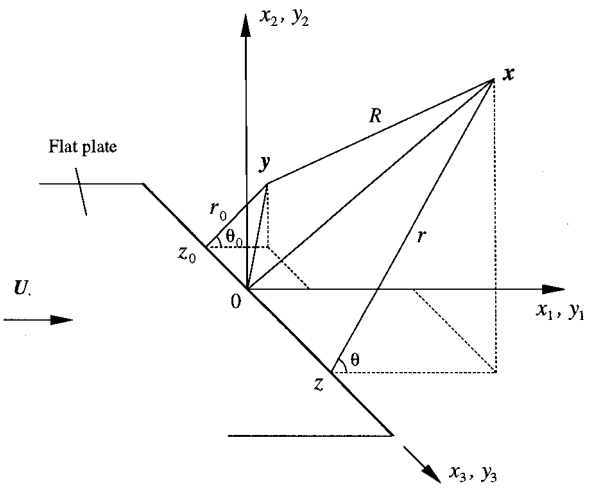

Fig. 9 Coordinate system for calculating the radiated noise of flow past the trailing edge of a semi-infinite thin plate.

independence of the volume integral), given the $(kr_0)^{-3/2}$ decay of the Green's function factor. A more general integral expression valid for all r_0 values has been derived in Ref. 28. However, calculations using both integrals show insignificant differences.

The noise calculation can be simplified further if the spanwise extent of the source field is acoustically compact ($z_0 \ll \lambda_a$). Although this is not generally the case for the full-span foil used in the experiment, it is valid for the source region contained within the

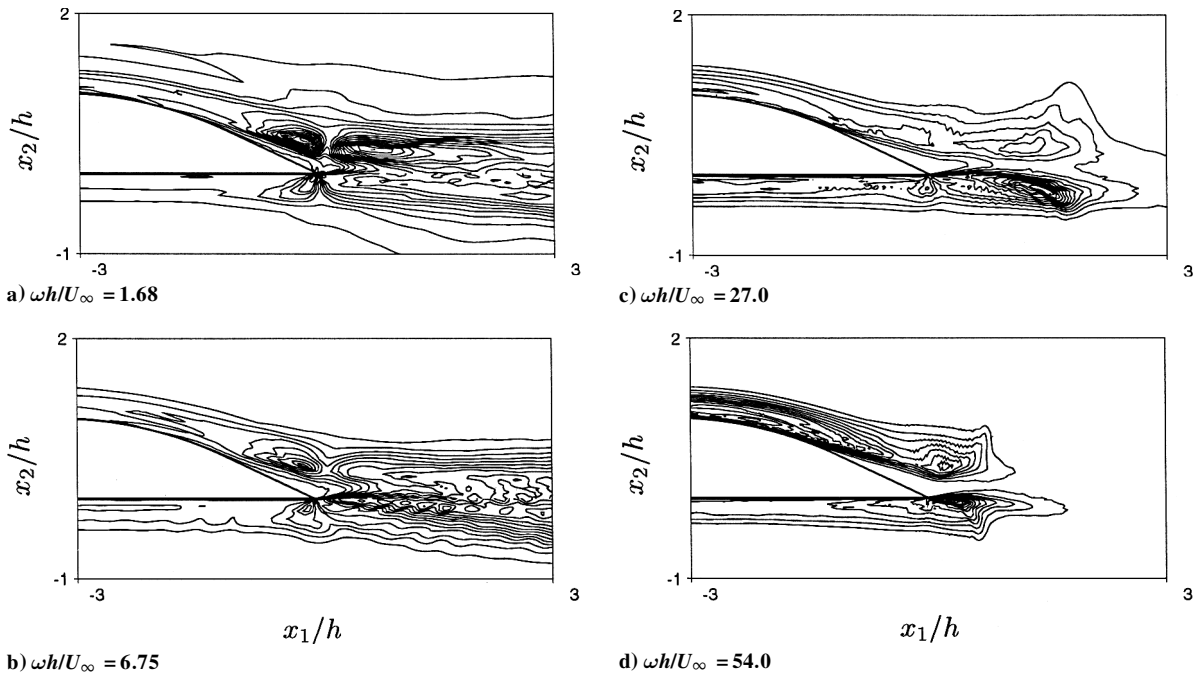

Fig. 10 Contours of the magnitude of the acoustic source term $-2\widehat{u_r u_\theta}/U_\infty^2$ at four different frequencies; contour levels ($\times 10^2$): a) 0.20–3.40, with increment 0.20; b) 0.20–3.00, with increment 0.20; c) 0.10–1.40, with increment 0.10; and d) 0.03–0.42, with increment 0.03.

computational domain (more discussion will follow in this regard). Equation (1) can then be approximated by

$$\hat{p}_a(\boldsymbol{x}, \omega) \approx \frac{\exp[i(k|\boldsymbol{x}| - \pi/4)]}{2^{\frac{5}{2}}\pi^{\frac{3}{2}}|\boldsymbol{x}|}(k \sin\phi)^{\frac{1}{2}} \sin\frac{\theta}{2}\,\hat{S}(\omega) \qquad (2)$$

where

$$S(t) = \int_V \frac{\rho_\infty}{r_0^{\frac{3}{2}}}\left\{\left(u_\theta^2 - u_r^2\right)\sin\frac{\theta_0}{2} - 2u_r u_\theta \cos\frac{\theta_0}{2}\right\} \mathrm{d}^3\boldsymbol{y} \qquad (3)$$

Equation (2) is particularly convenient to use because, rather than dealing with spatially distributed source terms, it involves only a single compact source $S(t)$ that can be easily evaluated during the source-field LES. Computations using Eqs. (1) and (2) again give nearly identical results for the low Mach number considered.

In the context of LES, the Lighthill stress is formally expressed as $\bar{T}_{ij} = \rho\bar{u}_i\bar{u}_j + \rho\tau_{ij}$, where the overline indicates spatial filtering and the entropy and viscous terms are ignored. It consists of nonlinear interactions among resolved scales (first term), and the subgrid scale contribution to the resolved scales (second term). Piomelli et al.[29] examined the effect of small scales on sound generation using a channel flow DNS database. In the present computation, the Lighthill stress terms are evaluated using the resolved velocity components only, assuming that the SGS contribution is relatively small. Note that the dynamic SGS model used in the source-field simulation gives only the anisotropic part of the SGS stress tensor, $\tau_{ij} - \delta_{ij}\tau_{kk}/3$, and, thus, the normal stress components cannot be determined. If one desires to include $\rho\tau_{ij}$ in the noise calculation, an alternative formulation of the SGS model, such as the dynamic localization model[30] that solves an additional equation for the SGS kinetic energy $\tau_{kk}/2$, should be used.

C. Results and Discussion

To compute the source terms in Eqs. (1) and (3), the velocity components u_1 and u_2 on the entire computational grid are sampled at every 10 time steps during the source-field LES. The sampling resolution $\Delta t_s U_\infty / h \approx 0.029$. The total record of $N = 1152$ time samples, covering a period $T_s U_\infty / h \approx 33.47$, is divided into eight segments with a 50% overlap. For each segment, which contains 256 samples, the source quantities $u_\theta^2 - u_r^2$ and $-2u_r u_\theta$ are computed, and the integral (3) is evaluated. The aperiodic time series are multiplied by the Hanning window function and discrete Fourier transforms are performed. The resulting Fourier coefficients are renormalized such that the power spectrum computed from them, when integrated over all positive frequencies, gives the mean-square fluctuations of the original function. If one deals with a span that is acoustically noncompact, then the Fourier transforms and the renormalization must be performed on the distributed source terms in Eq. (1) before the volume integration. As a result of the aforementioned procedure, eight sets of the source terms are available. Each set can be used in Eq. (2) [Eq. (1) if noncompact in span] to give a sample noise field, and the noise power spectra are obtained as the ensemble average of the spectra from all sample fields.

Figure 10 depicts the magnitude of the Reynolds shear-stress source term (normalized), $|-2\widehat{u_r u_\theta}|/U_\infty^2$, in the trailing-edgeregion at four selected frequencies. The other source term representing the normal stress behaves in a qualitatively similar manner. The source magnitudes are averaged over eight samples and the spanwise direction. The contour lines show that the spatial distribution of the acoustic source varies significantly with frequency. The low-frequency source, associated with the large-scale unsteady flow structures, exhibits strength in a large region including the wake (cf. Figs. 10a and 10b). The largest values are found in the shear layers emanating from the upper (separated) and lower (attached) boundary layers. As the frequency increases (Figs. 10c and 10d), the source distribution becomes more concentrated, particularly in the lower shear layer close to the trailing edge. The wake region farther from the edge contributes little to the high-frequency source terms due to a lack of the corresponding small-scale flow structures. In the convolution integrals (1) and (3), the source terms shown in Fig. 10 are weighted by an $r_0^{-3/2}$ factor, and, thus, the effective noise source is much more concentrated in the trailing-eddy region.

Trailing-edge noise from a source region consisting of the computational domain can be readily obtained from Eq. (1) or (2). In a typical LES, however, the spanwise width L_z of the computational domain is only a small fraction of the actual span L. For example, $L/L_z = 47$ for the present LES of Blake's experiment.[14] To predict the frequency spectrum of the sound pressure radiated from the entire span, one requires knowledge about the spanwise coherence of the source field. Kato et al.[4] discussed this issue in their calculation of noise from a cylinder wake. When we let $\Lambda_z = \Lambda_z(\omega)$ denote the coherence length for a given frequency, two limiting cases can be found for which the total noise is well defined:

1) If $L_z \geq \Lambda_z$, source regions separated by the computational box size radiate in a statistically independent manner. Hence, the total noise spectrum is the sum of contributions from L/L_z independent source regions along the span: $\Phi_{pa}^{\text{total}} \approx (L/L_z)\Phi_{pa}$.

2) If $L \leq \Lambda_z$, the source is coherent along the entire span (two-dimensional source). Based on Eq. (1), if the spanwise variation of the retarded time is ignored, $\hat{p}_a^{\text{total}} \approx (L/L_z)\hat{p}_a$, and, hence, $\Phi_{pa}^{\text{total}} \approx (L/L_z)^2\Phi_{pa}$.

In the intermediate regime $L_z < \Lambda_z < L$, and an accurate prediction of the total sound pressure is difficult to achieve. The computational domain is too small to accommodate the spanwise flow scales, and, thus, the acoustic source functions are not computed reliably. The rigorous remedy is to increase the computational box size L_z so that case 1 or 2 applies. This is, however, often extremely expensive. Kato et al.[4] resorted to an ad hoc approach in which Λ_z is approximated by extrapolating from the slowly decaying coherence function, and a hybrid formula based on cases 1 and 2 is used to estimate the total noise radiation.

Another ad hoc approach employed by previous investigators is the periodic extension of the computed source field to the entire span. The volume integral (1) is then taken over the expanded domain. This approach is essentially equivalent to the approach used in case 2, except that the integration takes into account retarded time variations along the span. Manoha et al.[13] used this method in their calculation of the noise from a blunt (rectangular) trailing edge of a flat plate.

In Fig. 11, several noise spectra are plotted as a function of frequency at $r/h = 150$, $z = 0$, and $M = 0.088$. Note that the normalization factor for the spectra includes Mach number dependence and directivity. The solid line is computed from the thin slab of the source field within the LES domain. The local spectrum peak near $\omega h/U_\infty = 23.6$ can be identified with the diffraction of boundary-layer eddies from the lower side. The total noise spectrum under the incoherent source assumption (case 1) is given by the dashed line, whereas the coherence source calculation (case 2) gives the chain-dashed line (the top curve). The latter serves as the upper bound of the true noise spectrum at low frequencies where condition 1 is invalid. The spectrum calculated using periodic source extension in x_3, shown as the dotted curve, coincides with that from the coherence-source calculation at low frequencies, and drifts to lower values at higher frequencies due to the increasing importance of retarded time variations. Nonetheless, it remains considerably larger than the spectrum level calculated under the incoherent source assumption, even in the wide frequency range where the assumption is perfectly valid (see discussions hereafter). This suggests that an acoustics calculation using a periodic source-domain extension will likely lead to overprediction of the total noise level.

A complete determination of the far-field noise requires the spanwise coherence of the source field to be computed. For a given field quantity q, the coherence is defined as

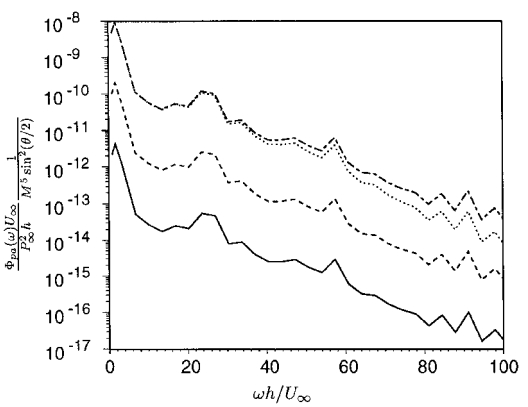

Fig. 11 Frequency spectra of the far-field noise at $r/h = 150$, $z = 0$, and $M = 0.088$: ——, spectrum calculated from a partial source field (the LES domain); - - - -, total spectrum assuming $L_z \geq \Lambda_z$; - - -, total spectrum assuming $L \leq \Lambda_z$; and · · · ·, total spectrum using periodic source extension in span.

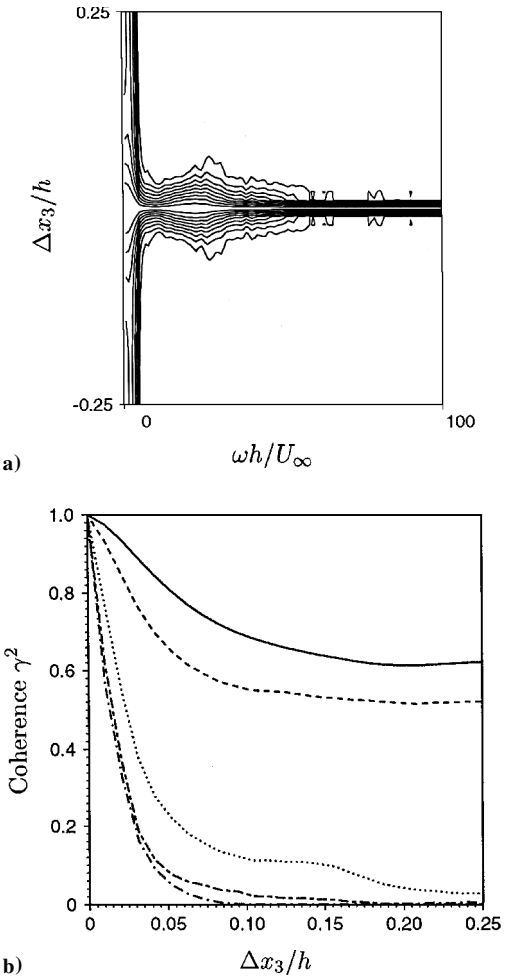

Fig. 12 Spanwise coherence of the fluctuating surface pressure on the upper surface near the trailing edge: a) contour plot (contour levels from 0.1 to 0.9, with increment 0.10) and b) coherence at frequencies $\omega h/U_\infty \approx$ 1.75 (——), 3.51 (- - - -), 5.26 (· · · ·), 7.01 (- - -), and 8.76 (- -·-).

$$\gamma^2(\boldsymbol{x}, \boldsymbol{r}, \omega) = \frac{|\Phi_{qq}(\boldsymbol{x}, \boldsymbol{r}, \omega)|^2}{|\Phi_{qq}(\boldsymbol{x}, 0, \omega)||\Phi_{qq}(\boldsymbol{x} + \boldsymbol{r}, 0, \omega)|} \tag{4}$$

where the cross spectrum function Φ_{qq} is the Fourier transform of the space–time cross correlation function

$$\Phi_{qq}(\boldsymbol{x}, \boldsymbol{r}, \omega) = \int_{-\infty}^{\infty} \langle q(\boldsymbol{x}, t) q(\boldsymbol{x} + \mathbf{r}, t + \tau) \rangle e^{-i\omega\tau}\, \mathrm{d}\tau \tag{5}$$

An estimate of γ^2 is made based on the fluctuating surface pressure ($q \equiv p$) in the vicinity of the trailing edge, under the premise that it is representative of the overall coherence of the volume distribution of source terms in Eq. (1). Figure 12 shows the spanwise pressure coherence on the upper surface, one-half grid spacing from the trailing edge. The upper plot shows the isocoherence contours as a function of frequency and spanwise separation. The coherence is seen to drop rapidly with spanwise separation, except at the low-frequency end. The coherence at selected low frequencies is depicted in the lower plot as a function of spanwise separation. It is observed that for $\omega h/U_\infty \geq 5.26$, the coherence exhibits sufficient drop within the computational domain, and, thus, $\Phi_{pa}^{\text{total}} \approx (L/L_z)\Phi_{pa}$ applies. The dashed curve in Fig. 11 gives the total noise spectrum. Thus, the present computational domain is adequate for the unique determination of the total noise over a fairly wide frequency range. Below the frequency $\omega h/U_\infty = 5.26$, however, the coherence length is larger than the spanwise dimension of the computational box, and the total noise cannot be determined with certainty. Given the flat shape of γ^2 at large separations shown in Fig. 12 (the solid and dashed lines), it is not possible to obtain the coherence lengths by extrapolation as in the case of Kato et al.[4]

The frequencies corresponding to $\lambda_a = C$ and h are given by $\omega h/U_\infty \approx 3.38$ and 71.4, respectively. They define the frequency range in which the half-plane Green's function is approximately valid. Outside this range other appropriate Green's functions should be used. In particular, when $\lambda_a \gg C$, the strut is acoustically compact, and, thus, the free-space Green's function is applicable. Curle's integral solution[2] to the Lighthill equation provides a more efficient tool for noise computation.[5]

The effect of finite chord (relative to acoustic wavelength), which is severe at low frequencies, can be inferred from the multiple-scattering analysis of Howe.[31] The finite chord is shown to cause the acoustic directivity to develop multiple lobes with radiation nulls in the directions $\theta = 0$ and π, as confirmed computationally by Singer et al.[10] Howe[31] observes that the departures from the half-plane radiation directivity (cardioid pattern) is particularly significant at reduced frequencies $kC < 10$, or $\omega h/U_\infty < 5.3$ in the present case. In addition, the noise spectrum level is expected to deviate significantly from the half-plane prediction for $\omega h/U_\infty < 1.2$, based on Howe's analysis.

At high frequencies ($\lambda_a \leq h$), the Green's function must, in principle, be tailored to the specific trailing-edge shape. However, the potential accuracy improvement is limited, given the relatively small tip angle of the edge and the competing high-frequency errors caused by the neglect of flow–acoustic interaction and SGS contribution to the acoustic source functions. Additional errors may arise from the finite foil thickness relative to the source-field dimension, even when the foil is acoustically thin. This affects the source strength for a wider frequency range but does not fundamentally alter the radiation characteristics (directivity and velocity scaling). In recent studies, Howe[26,27] shows that the error arising from the half-plane approximation is significant at high frequencies, when the boundary layer responsible for noise generation separates near the trailing edge. The high-frequency sound in the present study is generated predominantly by the interaction of the attached boundary layer (on the lower side) with the trailing edge and is thus minimally impacted by the simplified Green's function. If more accurate solutions are desired, a shape-dependent Green's function for an acoustically thin foil should be employed, which can be obtained computationally following the analysis of Howe.[26,27]

As pointed out earlier, Blake's experiment[14] does not include acoustic measurements, and, thus, a direct comparison with the numerical predictions cannot be made. As a qualitative assessment, the acoustic pressure spectra measured in a different experiment by Blake and Gershfeld[7] are plotted in Fig. 13 along with the simulation data at $r/h = 33$, $\theta = \pi/2$, and $z = 0$. The normalization used in Fig. 13 follows that of Ref. 7, where y_f ($\approx 0.2h$ from the simulation) is the minimum distance between the shear layers in the wake and M_c (approximated by 0.72 M in the calculation) is the convective Mach number of turbulence past the trailing edge. The experimental measurements, obtained for $9 \times 10^3 \leq Re_{y_f} \leq 3.6 \times 10^4$ (the Reynolds number is based on y_f and U_∞), are represented by the shaded area.

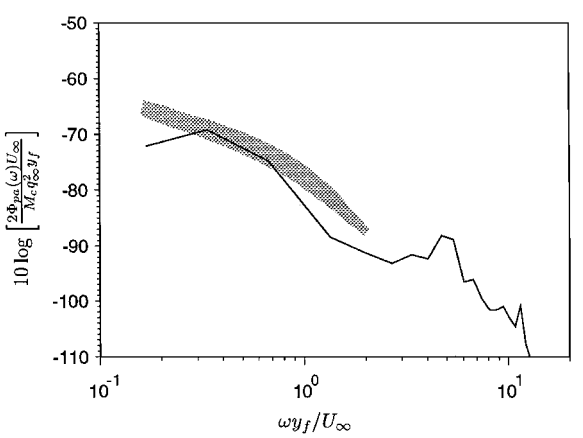

Fig. 13 Comparison of the computed noise spectrum (——) with the measurements of Blake and Gershfeld[7] (shaded area) at $r/h = 33$, $\theta = \pi/2$, and $z = 0$; experimental data were obtained for $9 \times 10^3 \leq Re_{y_f} \leq 3.6 \times 10^4$.

They are found to be concentrated at relatively low frequencies and compare rather favorably with the computed spectrum, which is based on the incoherence-source ($L_z \geq \Lambda_z$) assumption and has been adjusted for the larger span ($=48h$) used in the experiment. Of course, the incoherence-source assumption is formally valid only for $\omega y_f/U_\infty \geq 1.05$ (cf. Fig. 12), and, hence, much of the quantitative agreement (or disagreement) shown in Fig. 13 needs to be discounted. The comparison should be interpreted in a qualitative sense. Aside from differences in trailing-edge shape and flow conditions between the simulation and the experiment, certain additional assumptions used in the acoustics calculations, including the long-chord (relative to wavelength) and far-field approximations, are also violated in the low-frequency regime.

Finally, note that an important issue in edge-noise theory is the applicability of the unsteady-flow Kutta condition. As shown by Howe,[11] models based on potential flow theory with and without imposing the Kutta condition can give sound-pressure level predictions that differ by 10 dB or more. Because the present work is based on numerical solutions to the viscous Navier–Stokes equations, no such ambiguity exists, and, hence, no special treatment is needed at the trailing edge. Highly accurate DNS and LES calculations can help clarify the precise conditions prevailing at the trailing edge. This will be pursued in future investigations.

IV. Summary

An LES has been carried out for turbulent boundary-layer flows past an asymmetrically beveled trailing edge of a flat strut at a chord Reynolds number of 2.15×10^6. The asymmetric edge of 25-deg tip angle produces a separated boundary layer on one side and an attached boundary layer on the other. The computed mean and fluctuating velocity profiles compare reasonably well with the experimental measurements of Blake.[14] The discrepancies observed at some stations may have been caused by inadequate inflow velocity conditions, small computational domain size, as well as possible experimental errors near the wall and inside the separated region.

The objectives of the trailing-edge flow LES are to predict the space–time characteristics of surface pressure fluctuations and to provide the acoustic source functions for the far-field noise calculation. The frequency spectra of surface pressure fluctuations obtained from LES agree well with experimental measurements at most stations. The cause for the over-prediction at station G needs to be further investigated. The space–time correlations of the fluctuating surface pressure demonstrate a dramatic increase in temporal and spanwise spatial scales beneath the unsteady separation region. The correlation functions near the trailing-edge show insufficient drop at maximum spanwise separations, suggesting the need for a wider computational domain.

The far-field acoustics is computed from an integral-form solution to the Lighthill equation developed by Ffowcs-Williams and Hall.[8] The Green's function is approximated by that for an infinitely thin half-plane, given the thin foil (relative to acoustic wavelength) and the small included angle of the trailing edge. The acoustic evaluation is performed in the Fourier frequency domain using source-field data obtained from LES. Computations have been carried out to determine the source-term characteristics and the far-field noise spectra. To predict accurately the noise radiation from the entire span using a partial source field included in the LES domain, the spanwise domain size is required to be larger than the coherence length of the source field in that direction. The present LES domain is found to be adequate for predicting noise radiation over a range of frequencies. At low frequencies, however, the spanwise source coherence estimated based on surface pressure fluctuations does not decay sufficiently. This issue will be addressed in future simulations using an expanded computational domain.

Acknowledgments

This work was supported by the U.S. Office of Naval Research under Grant N00014-95-1-0221. Computations were carried out on facilities at the U.S. Department of Defense Major Shared Resource Center/Aeronautical Systems Center. We gratefully acknowledge William K. Blake, Peter Bradshaw, Thomas S. Lund, and Rajat Mittal for valuable discussions during the course of this

work, and an anonymous referee for the many constructive suggestions. Preliminary versions of this work were presented at the 3rd ASME/JSME Joint Fluids Engineering Conference, FEDSM99-7231, San Francisco, California, 18–23 July 1999, and the Workshop on Industrial and Environmental Applications of Direct and Large-Eddy Simulation, Bogazici University, Istanbul, Turkey, 5–7 August 1998.

References

[1]Lighthill, M. J., "On Sound Generated Aerodynamically: I. General Theory," *Proceedings of the Royal Society of London, Series A*: *Mathematical and Physical Sciences*, Vol. 211, No. 1107, 1952, pp. 564–587.

[2]Curle, N., "The Influence of Solid Boundaries Upon Aerodynamic Sound," *Proceedings of the Royal Society of London, Series A*: *Mathematical and Physical Sciences*, Vol. 231, No. 1187, 1955, pp. 505–514.

[3]Ffowcs-Williams, J. E., and Hawkings, D. L., "Sound Generation by Turbulence and Surfaces in Arbitrary Motion," *Philosophical Transactions of the Royal Society of London, Series A*: *Mathematical and Physical Sciences*, Vol. 264, No. 1151, 1969, pp. 321–342.

[4]Kato, C., Iida, A., Takano, Y., Fujita, H., and Ikegawa, M., "Numerical Prediction of Aerodynamic Noise Radiated from Low Mach Number Turbulent Wake," AIAA Paper 93-0145, Jan. 1993.

[5]Wang, M., Lele, S. K., and Moin, P., "Computation of Quadrupole Noise Using Acoustic Analogy," *AIAA Journal*, Vol. 34, No. 11, 1996, pp. 2247–2254.

[6]Brooks, T. F., and Hodgson, T. H., "Trailing Edge Noise Prediction from Measured Surface Pressures," *Journal of Sound and Vibration*, Vol. 78, No. 1, 1981, pp. 69–117.

[7]Blake, W. K., and Gershfeld, J. L., "The Aeroacoustics of Trailing Edges," *Frontiers in Experimental Fluid Mechanics*, edited by M. Gad-el-Hak, Springer-Verlag, New York, 1988, Chap. 10, pp. 457–532.

[8]Ffowcs-Williams, J. E., and Hall, L. H., "Aerodynamic Sound Generation by Turbulent Flow in the Vicinity of a Scattering Half Plane," *Journal of Fluid Mechanics*, Vol. 40, 1970, pp. 657–670.

[9]Crighton, D. G., and Leppington, F. G., "On the Scattering of Aerodynamic Noise," *Journal of Fluid Mechanics*, Vol. 46, 1971, pp. 577–597.

[10]Singer, B. A., Brentner, K. S., Lockard, D. P., and Lilley, G. M., "Simulation of Acoustic Scattering from a Trailing Edge," AIAA Paper 99-0231, Jan. 1999.

[11]Howe, M. S., "A Review of the Theory of Trailing Edge Noise," *Journal of Sound and Vibration*, Vol. 61, No. 3, 1978, pp. 437–465.

[12]Blake, W. K., *Mechanics of Flow-Induced Sound and Vibration*, Vols. 1 and 2, Academic, London, 1986.

[13]Manoha, E., Troff, B., and Sagaut, P., "Trailing-Edge Noise Prediction Using Large-Eddy Simulation and Acoustic Analogy," *AIAA Journal*, Vol. 38, No. 4, 2000, pp. 575–583.

[14]Blake, W. K., "A Statistical Description of Pressure and Velocity Fields at the Trailing Edge of a Flat Strut," David Taylor Naval Ship Research and Development Center, Rept. 4241, Bethesda, MD, Dec. 1975.

[15]Germano, M., Piomelli, U., Moin, P., and Cabot, W. H., "A Dynamic Subgrid-Scale Eddy Viscosity Model," *Physics of Fluids A*, Vol. 3, No. 7, 1991, pp. 1760–1765.

[16]Lilly, D. K., "A Proposed Modification of the Germano Subgrid Scale Closure Method," *Physics of Fluids A*, Vol. 4, No. 3, 1992, pp. 633–635.

[17]Choi, H., "Toward Large Eddy Simulation of Turbulent Flow over an Airfoil," *Annual Research Briefs—1993*, Center for Turbulence Research, Stanford Univ./NASA Ames Research Center, Stanford, CA, 1993, pp. 145–149.

[18]Mittal, R., "Progress on LES of Flow Past a Circular Cylinder," *Annual Research Briefs—1996*, Center for Turbulence Research, Stanford Univ./NASA Ames Research Center, Stanford, CA, 1996, pp. 233–241.

[19]Menter, F. R., "Zonal Two-Equation k–ω Turbulence Models for Aerodynamic Flows," AIAA Paper 93-2906, Jan. 1993.

[20]Lund, T. S., Wu, X., and Squires, K. D., "Generation of Turbulent Inflow Data for Spatially-Developing Boundary Layer Simulations," *Journal of Computational Physics*, Vol. 140, No. 2, 1998, pp. 233–258.

[21]Pauley, L. L., Moin, P., and Reynolds, W. C., "The Structure of Two-Dimensional Separation," *Journal of Fluid Mechanics*, Vol. 220, 1990, pp. 397–411.

[22]Mittal, R., and Moin, P., "Suitability of Upwind-Biased Finite Difference Schemes for Large-Eddy Simulation of Turbulence Flows," *AIAA Journal*, Vol. 35, No. 8, 1997, pp. 1415–1417.

[23]Kaltenbach, H.-J., Fatica, M., Mittal, R., Lund, T. S., and Moin, P., "Study of Flow in a Planar Asymmetric Diffuser Using Large-Eddy Simulation," *Journal of Fluid Mechanics*, Vol. 390, 1999, pp. 151–185.

[24]Wang, M., "LES with Wall Models for Trailing-Edge Aeroacoustics," *Annual Research Briefs—1999*, Center for Turbulence Research, Stanford Univ./NASA Ames Research Center, Stanford, CA, 1999, pp. 355–364.

[25]Bradshaw, P., *An Introduction to Turbulence and Its Measurement*, Pergamon, Oxford, 1971.

[26]Howe, M. S., "Trailing Edge Noise at Low Mach Numbers," *Journal of Sound and Vibration*, Vol. 225, No. 2, 1999, pp. 211–238.

[27]Howe, M. S., "Trailing Edge Noise at Low Mach Numbers, Part 2: Attached and Separated Edge Flows," *Journal of Sound and Vibration*, Vol. 234, No. 5, 2000, pp. 761–775.

[28]Wang, M., "Towards Numerical Simulations of Trailing-Edge Aeroacoustics," *Annual Research Briefs—1996*, Center for Turbulence Research, Stanford Univ./NASA Ames Research Center, Stanford, CA, 1996, pp. 133–142.

[29]Piomelli, U., Streett, C. L., and Sarkar, S., "On the Computation of Sound by Large-Eddy Simulation," *Journal of Engineering Mathematics*, Vol. 32, 1997, pp. 217–236.

[30]Ghosal, S., Lund, T. S., Moin, P., and Akselvoll, K., "A Dynamic Localization Model for Large-Eddy Simulation of Turbulent Flows," *Journal of Fluid Mechanics*, Vol. 286, 1995, pp. 229–255.

[31]Howe, M. S., "Edge-Source Acoustic Green's Function for an Airfoil of Arbitrary Chord, with Application to Trailing-Edge Noise," *Quarterly Journal of Mechanics and Applied Mathematics* (to be published).

M. Samimy
Associate Editor